INTERNATIONAL JOURNAL OF HYDROGEN ENERGY XXX (2017) 1–12

Available online at www.sciencedirect.com

ScienceDirect

journal homepage: www.elsevier.com/locate/he

A combined experimental and computational study of water-gas shift reaction over rod-shaped $Ce_{0.75}M_{0.25}O_2$ (M = Ti, Zr, and Mn) supported Cu catalysts

Zhibo Ren [a,b], *Fei Peng* [a], *Biaohua Chen* [a], *Donghai Mei* [b,**], *Jianwei Li* [a,*]

[a] *State Key Laboratory of Chemical Resource Engineering, Bejing University of Chemical Technology, Beijing 100029, PR China*

[b] *Institute for Integrated Catalysis, Pacific Northwest National Laboratory, Richland, WA, 99352, United States*

ARTICLE INFO

Article history:
Received 22 August 2017
Received in revised form
5 October 2017
Accepted 8 October 2017
Available online xxx

Keywords:
Mixed ceria nanorods
Cu catalysts
Water-gas shift reaction
Cu-support interaction
DFT calculation

ABSTRACT

Water-gas shift (WGS) reaction over a series of ceria-based mixed oxides supported Cu catalysts was investigated using a combined experimental and theoretical method. The mixed rod-shaped $Ce_{0.75}M_{0.25}O_2$ (M = Ti^{4+}, Zr^{4+}, Mn^{4+}) solid solutions, which majorly expose the (110) and (100) facets, are synthesized by hydrothermal method and used to prepare supported Cu catalysts. It is found that the Cu/$Ce_{0.75}Ti_{0.25}O_2$ (Cu-CT) exhibits the highest CO conversion in the temperature range of 150–250 °C among all supported Cu catalysts. This is mainly attributed to (i) good dispersion of Cu; (ii) largest amount of moderate copper oxide; and (iii) strongest Cu-support interaction of Cu-CT. Compared to other mixed metals, periodic density functional theory calculations performed in this work further suggest that the introduction of Ti into CeO_2 not only promotes oxygen vacancy formation and CO adsorption, but also facilitates the carboxyl (COOH) formation at the interface of the Cu cluster and the support, which leads to the enhanced catalytic activity of the Cu-CT toward WGS reaction.

© 2017 Hydrogen Energy Publications LLC. Published by Elsevier Ltd. All rights reserved.

Introduction

The proton exchange membrane fuel cells (PEMFC) have attracted considerable attention as a promising device to generate power for stationary and mobile applications [1]. Among various fuels, hydrogen is considered to be the ideal feedstock for the PEMFC due to its high power capacity and environmental benign nature. Currently, hydrogen is mainly produced from the reforming of crude oil, coal, natural gas, and biomass resources. However, the reformate gas generally contains 1–10 vol% CO, which can poisons Pt catalyst used as the anode in PEMFC [2]. To remove CO and produce more hydrogen fuel, water-gas shift (WGS) reaction ($CO + H_2O \rightarrow CO_2 + H_2$) is generally carried out in the fuel preprocessor of PEMFC. Hence, there is an urgent need to develop more efficient and high selectivity WGS catalysts [3].

* *Corresponding author.*
** *Corresponding author.*
E-mail addresses: donghai.mei@pnnl.gov (D. Mei), lijw@mail.buct.edu.cn (J. Li).

https://doi.org/10.1016/j.ijhydene.2017.10.047

0360-3199/© 2017 Hydrogen Energy Publications LLC. Published by Elsevier Ltd. All rights reserved.

Please cite this article in press as: Ren Z, et al., A combined experimental and computational study of water-gas shift reaction over rod-shaped $Ce_{0.75}M_{0.25}O_2$ (M = Ti, Zr, and Mn) supported Cu catalysts, International Journal of Hydrogen Energy (2017), https://doi.org/10.1016/j.ijhydene.2017.10.047

Cu-based catalysts have been considered to be one of most promising catalysts for WGS reaction due to its high activity, stability and economical availability [4]. It is well known that the catalytic performance of Cu based WGS catalysts is closely related to the dispersion of copper oxide species, which is significantly affected by the support materials [5,6]. Various oxides such as CeO_2 [7,8], Al_2O_3 [9], and ZrO_2 [10,11] have been chosen as the support for copper catalyst. Among those oxides, CeO_2 has received considerable attention due to its high oxygen storage capacity (OSC) and strong interaction with active metal [8]. Recent theoretical and experimental studies indicate that the specific chemical and physical properties of exposed facets play an essential role in determining catalytic properties of CeO_2 with controlled morphologies [12]. CeO_2 nanorods with majorly exposed (100) and (110) facets were reported as excellent supports for a range of reactions, including CO oxidation [13], NO reduction [14], ammonia synthesis [15], and WGS [16]. This is mainly due to the high oxygen mobility over the (110) facet of CeO_2 nanorods and the strong metal-CeO_2 interaction that facilitates stabilizing and anchoring active metal centers [17].

Ceria can easily form solid solutions with transition metal (M) ions, such as Zr^{4+}, Ti^{4+}, and Mn^{4+}. CeO_2-based mixed solid solutions have attracted great attentions due to their outstanding textural properties, improved OSC and redox properties in comparison with pure CeO_2 [18–21]. Jeong et al. synthesized a series of Cu-$Ce_xZr_{1-x}O_2$ catalysts, which were applied for low temperature WGS reaction [19]. It was found that Cu-$Ce_{0.8}Zr_{0.2}O_2$ with Ce/Zr ratio of 4 showed the highest CO conversion. Petallidou et al. reported that $Ce_{0.8}Ti_{0.2}O_{2-\delta}$ supported Pt catalysts exhibited much higher specific WGS reaction rate than that of pure TiO_2 or CeO_2 [21]. Fraccari et al. prepared a series of mixed Ce-Mn oxides as the support for Cu and Ni catalysts [18]. Compared to pure ceria or manganese oxides, the mixed Ce-Mn oxide displayed superior activity for WGS reaction. These previous work mainly focused on the catalytic property of the catalyst by modulating the ratio of Ce/M. However, a systematic and comparative study of the rod-shaped ceria-based mixed solid solutions supported Cu catalyst for WGS reaction has not been reported yet.

In this work, a series of $Ce_{0.75}M_{0.25}O_2$ ($M = Ti^{4+}$, Zr^{4+}, Mn^{4+}) solid solutions (Ce:M = 3:1 M ratio) were prepared by a two-step hydrothermal method. Cu-$Ce_{0.75}M_{0.25}O_2$ catalysts for WGS reaction were further prepared by deposition precipitation approach. In particular, the effects of the second metal introduction into CeO_2 on the dispersion of Cu catalysts, the Cu-support interaction, and catalytic performance were investigated. Finally, DFT calculations were employed to gain fundamental insight into the roles of mixing second metals in WGS reaction.

Experimental and computational methods

Catalyst preparation

Preparation of supports

The CeO_2 nanorods were synthesized by a hydrothermal method as previously reported [16]. The cerium nitrate precursor ($Ce(NO_3)_3.6H_2O$, 4 mmol) was firstly dissolved in 80 ml aqueous NaOH solution (6 M) under stirring. Then, the mixture was introduced into a stainless steel autoclave and kept at 100 °C for 24 h. After that, the precipitants were separated and washed with deionized water and ethanol to remove ionic residues. The CeO_2 nanorods could be obtained after being dried at 100 °C overnight and calcined in air at 400 °C for 4 h.

Rod-shaped $Ce_{0.75}M_{0.25}O_2$ ($M = Ti^{4+}$, Zr^{4+}, Mn^{4+}) mixed oxides were synthesized following the procedure reported in the literature [22]. The as calcined CeO_2 nanopowders were added into deionized water under stirring. The mixed metal precursor was dissolved in deionized water and added into the above CeO_2 solution dropwise. The mixture was introduced into a stainless steel autoclave and kept at 180 °C for 24 h. These synthesized samples were the $Ce_{0.75}Ti_{0.25}O_2$, $Ce_{0.75}Zr_{0.25}O_2$ and $Ce_{0.75}Mn_{0.25}O_2$ solid solutions, which hereafter were denoted as CT, CZ and CM in this work, respectively.

Preparation of catalysts

The Cu-$Ce_{0.75}M_{0.25}O_2$ catalysts were prepared by a deposition-precipitation method [23]. The prepared CeO_2, CT, CZ, and CM were used as support materials and the copper nitrate solution (50%) was used as the source of copper. The copper loading was selected as 5 wt%. The obtained catalysts were denoted as Cu-CeO_2, Cu-CT, Cu-CZ and Cu-CM, respectively.

Catalyst characterization

The powder X-ray powder diffraction (XRD) was performed on an X-ray diffractometer with Cu-Kα radiation (D8FOCUS, Bruker, Germany). The average crystallite size of sample was determined from the peak broadening with the Scherrer equation. The morphology and size of the samples were characterized on a transmission electron microscope (TEM) (JEM-2010, JEOL, Japan). The specific surface area (S_{BET}) of the sample was measured in an automated sorption instrument (Sorptomatic 1990, Thermo Electron, USA) through nitrogen adsorption/desorption at 77 K, which was calculated by the Brunauer-Emmett-Teller (BET) method. The UV-vis spectroscopy was obtained by an Ultraviolet visible near infrared spectrophotometer (UV-3600, Shimadzu, Japan). X-ray photoelectron spectroscopy (XPS) was conducted on a photoelectron spectrometer with Al Kα radiation (ESCALAB 250, Thermofisher, USA) under ultrahigh vacuum (UHV), calibrated internally by carbon deposit C (1s) having a binding energy (BE) at 284.6 eV.

H_2-temperature programmed reduction (TPR) was performed using Thermo Electron TPD/R/O 1100 Series instrument (Thermo Electron, USA) equipped with a thermal conductivity detector (TCD). A quartz Utube reactor was loaded with 0.10 g of the sample and was then pretreated under Ar atmosphere (30 mL min^{-1}) at 100 °C for 1 h. The H_2 TPR was performed using 10 vol% of H_2/Ar at a flow rate of 30 mL min^{-1} in the temperature range 100–500 °C at a heating rate of 10 °C·min^{-1}. The effluent stream was introduced into a water trap filed with blue silica gel to remove moisture before it reached the TCD.

In situ Fourier Transform Infrared Spectroscopy (FTIR) experiments were conducted on a FTIR spectrometer (TENSOR 27, Bruker, Germany) equipped with a MCT detector and a

Please cite this article in press as: Ren Z, et al., A combined experimental and computational study of water-gas shift reaction over rod-shaped $Ce_{0.75}M_{0.25}O_2$ (M = Ti, Zr, and Mn) supported Cu catalysts, International Journal of Hydrogen Energy (2017), https://doi.org/10.1016/j.ijhydene.2017.10.047

diffuse reflection accessory including a temperature controllable reaction cell. After the sample was placed into the reaction cell under He flow (20 mL min^{-1}), the temperature was raised to 200 °C. As the background spectrum was collected and the baseline of spectrum was stabilized, the He flow was cut off and the stream of CO/He (5 vol% CO) was introduced into the cell. IR spectra were recorded by accumulating 64 scans at a spectrum resolution of 4 cm^{-1}.

Evaluation of catalytic performance

The WGS reaction activities of the catalysts were tested in a fixed bed reactor at atmospheric pressure and in the temperature range of 150–350 °C at an interval of 50 °C. In the present work, 0.2 g of catalyst was used and the space velocity was 6000 h^{-1}. The typical feed reformate gas contained 10 vol % CO, 70 vol% H_2, 10 vol% CO_2 and balanced with N_2; the ratio of vapor to feed gas was maintained at 1:1. The residual water of the outlet was removed by a condenser before entering a gas chromatograph equipped with a TCD. The activity is expressed by the conversion of CO (X_{CO}), defined as:

$$X_{CO} = \frac{1 - [CO]_{in}/[CO]_{out}}{1 + [CO]_{out}} \times 100\% \quad (1)$$

where $[CO]_{in}$ and $[CO]_{out}$ are the inlet and outlet concentrations of CO. The WGS reaction rates were measured using eq (2) in separate experiments where the conversion of CO was kept below 20%. As such, differential reaction conditions could be assumed with negligible heat and mass-transfer effects.

$$r_{CO} = \frac{F_{CO} X_{CO}}{W_{cat}} \quad (2)$$

where r_{CO} is the conversion rate of CO ($mol \cdot g^{-1} \cdot s^{-1}$), F_{CO} is the molar flow rate of CO into the reactor ($mol \cdot s^{-1}$), and W_{cat} is the mass of the catalysts (g).

Computational details

All periodic DFT calculations were performed using the Vienna ab initio Simulation Package (VASP) [24,25]. The electron exchange and correlation were treated within the generalized gradient approximation (GGA) using the Perdew-Burke-Ernzerhof (PBE) functional [26]. The core electrons of all the atoms were described by the projector-augmented wave (PAW) pseudopotential with a cut-off energy of 400 eV. DFT + U correction was used for the description of Ce 4f-orbitals with the value of U = 5 eV [27]. The CeO_2(110) surface was modeled by a p(2 × 2) unit cell with 6 atomic layers and the mixed surface was constructed by substituting Ce cations with M metals. During optimization, the bottom three layers were fixed, while the other layers and adsorbates were allowed to relax. The k-points sampling was generated by the Monkhorst Pack procedure with a (3 × 3 × 1) mesh and a 15 Å vacuum was introduced to eliminate the interaction between neighboring slabs. The electronic self-consistent field was converged to 10^{-5} eV and the forces on all atoms were converged to less than 0.02 eV/Å. Spin polarization was considered in all calculations. The adsorption energy was calculated as follows:

$$E_{ads} = E_{adsorbate/slab} - E_{slab} - E_{adsorbate} \quad (3)$$

where $E_{adsorbate/slab}$ is the total energy of adsorbate/slab system, E_{slab} is the total energy of the clean slab and $E_{adsorbate}$ is the total energy of adsorbate in vacuum. The vibrational frequencies of the adsorbed CO were calculated in the harmonic approximation. The Hessian matrix was constructed using the finite difference method, where atoms are displaced by 0.02 Å along each direction of the three Cartesian coordinates. The transition states (TS) of surface reactions were searched using the climbing-image nudged elastic band method [28]. The activation energy was determined as the energy difference between the corresponding TS and initial states (IS) and the reaction energy was defined as the corresponding final states (FS) and IS energy difference.

Results and discussion

Structural characterization of the catalysts

The XRD patterns of the support materials and the Cu catalysts are shown in Fig. 1. For all support materials, only the broad diffraction patterns at 2θ of 28.68, 33.22, 47.58, 56.42, and 59.22, which are attributed to a cubic fluorite-type phase CeO_2 (PDF-ICDD 34-0394), are detected without extra characteristic patterns assigned to ZrO_2, TiO_2 and MnO_2. Furthermore, the diffraction peaks of CZ, CT and CM are slightly shifted to the high angle direction with respect to that of CeO_2, indicating that Ti^{4+}, Zr^{4+} and Mn^{4+} have been successfully incorporated into the lattice of CeO_2 to form uniform mixed solid solutions, whilst maintaining the typical fluorite-type structure. After the introduction of copper oxide species, the support materials remain in the initial face-centered cubic structure without appearance of crystalline of CuO. This indicates that copper oxide species are highly dispersed and/or present as very small clusters being difficult to be detected due to limitation of XRD.

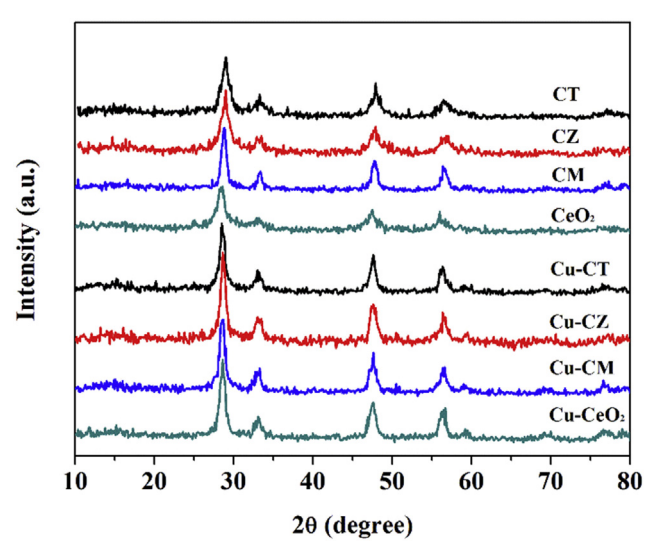

Fig. 1 – The powder XRD patterns of supports and Cu-based catalysts.

Please cite this article in press as: Ren Z, et al., A combined experimental and computational study of water-gas shift reaction over rod-shaped $Ce_{0.75}M_{0.25}O_2$ (M = Ti, Zr, and Mn) supported Cu catalysts, International Journal of Hydrogen Energy (2017), https://doi.org/10.1016/j.ijhydene.2017.10.047

The cell parameters of the oxide supports calculated by XRD are listed in Table 1. It is found that the lattice parameters of CZ, CT and CM are smaller than that of CeO_2. This is primarily due to the fact that the ionic radius of Zr^{4+} (0.80 Å), Ti^{4+} (0.68 Å) and Mn^{4+} (0.53 Å) is smaller than that of Ce^{4+} (0.92 Å) [29,30], and incorporation of Zr^{4+}, Ti^{4+} and Mn^{4+} into the CeO_2 lattice can lead to a certain contraction and distortion of the lattice. The mean crystallite sizes of the supports determined by Debye-Scherrer equation based on diffraction peak of (111) are listed in Table 1. The calculated sizes suggest that the grain size of these ceria-based solid solutions is generally smaller than that of CeO_2. This phenomenon is due to the surface reconstruction of samples in the second hydrothermal process. In addition to that, the BET specific surface areas of the supported Cu catalysts slightly increase after the introduction of these foreign metal cations (see Table 1).

The morphologies of the supports as well as supported Cu catalysts were investigated by TEM, as shown in Fig. 2a and Fig. S1. The one dimension rod-like structure with a preferred growth along [110] crystallographic direction is clearly observed for the pre-synthesized CeO_2 and $Ce_{0.75}M_{0.25}O_2$ (Zr^{4+}, Ti^{4+}, Mn^{4+}) solid solutions. Elemental mapping (Fig. 2a inset) illustrates that the mixed Ti^{4+} are homogenously distributed within the CeO_2 host structure. It has been reported that these nanorods are predominantly exposed the (110) and (100) planes [22]. With controlled crystalline morphology and composition, the obtained mixed CeO_2 samples provide an ideal platform to correlate the support composition with catalytic performance. It is worth noting that the rod-shaped structures of $Ce_{0.75}M_{0.25}O_2$ (Zr^{4+}, Ti^{4+}, Mn^{4+}) are shorter than that of CeO_2 (See Fig. S1), which is due to the second hydrothermal treatment of $Ce_{0.75}M_{0.25}O_2$ (Zr^{4+}, Ti^{4+}, Mn^{4+}) samples. The conversion from the as-synthesized long CeO_2 rods to short mixed rods would account for the increase of BET surface and the decrease of crystallite size. The TEM images of Cu-$Ce_{0.75}M_{0.25}O_2$ (Fig. S1) show that the rod-like shaped supports still inherit their authentic morphologies after deposition of Cu. CuO particles are not distinguished from the TEM images due to low contrast between Cu and Ce, and the high dispersion of minute particles.

Information on the surface coordination and electronic states of the metal ions were obtained from the UV-vis measurement. As shown in Fig. 3a, all these supports exhibit two adsorption bands at about 271 and 347 nm, which could be attributed to O^{2-}–Ce^{4+} charge transfer and interband transitions, respectively [31]. However, the absorption band at 255 nm corresponding to an O^{2-}–Ce^{3+} charge transfer is not clearly observed. Furthermore, it can be seen that the adsorption edges of mixed supports differ from that of CeO_2. The shift of adsorption edge means change of the band gap, which is result of incorporation of Zr^{4+}, Ti^{4+} and Mn^{4+} into the lattice of CeO_2 leading to a decrease of symmetry and consequently the strain development at the cerium sites. It is noted that the adsorption bands of ZrO_2, TiO_2 and MnO_2 are not detectable due to the introduction of foreign metal atoms into the lattice of CeO_2 [30], which is in good agreement with XRD and TEM results. The spectra of investigated supported Cu catalysts are shown in Fig. 3b. An absorption band can be detected at 475 nm, which is assigned to Cu^{+} clusters and/or bis(μ-oxo)dicopper core ($[Cu_2O]^{2+}$) [32]. All supported Cu catalysts show a broad d–d transition band of Cu^{2+} ions in the visible region [33]. These bands show a shift from 722 to 770 nm with a change in supports. It is well known that the difference in the peak intensity generally depends on ion density and the chemical environment. Therefore, these results verify presence of different Cu species, which indicates that incorporation of different foreign metal atoms into lattice of CeO_2 could result in different coordination environments of the supported copper oxide.

The surface composition and elemental oxidation states of the catalysts was studied by XPS, as shown in Fig. 4. The XPS spectrum of Ce 3d is numerically fitted with eight components for each sample, and the corresponding assignments are defined in Fig. 4a. The two groups of spin-orbital multiplets attributing to $3d_{3/2}$ and $3d_{5/2}$ are denoted as u and v, which are extending in the binding energy range of 880–920 eV [8]. It has been widely reported that the bands labeled as u and v, u'' and v'', u''' and v''' are assigned to Ce^{4+}, while the bands of u' and v' are related to Ce^{3+}, indicating the generation of oxygen vacancies. As a result, the chemical valence state of cerium on the surface of these cerium-containing samples is mainly in a +4 oxidation state, and a small part of Ce^{3+} co-exists, which is consistent with the UV-vis results. A high Ce^{3+} content is found in the Cu-CT (14.1%), Cu-CZ (13.6%) and Cu-CM (12.5%), while in Cu-CeO_2 only 11.0% of Ce^{3+} is present (see Table 1). It is worth noting that the ratio of $Ce^{3+}/(Ce^{3+}+Ce^{4+})$ on the surface of these samples is enhanced by the incorporation of Ti^{4+}, Zr^{4+} and Mn^{4+} into the CeO_2 lattice and thus more oxygen vacancies exist on support surface.

As shown in Fig. 4b, the as-prepared catalysts exhibit the typical XPS spectra of Cu^{2+} with Cu $2p_{3/2}$ and $2p_{1/2}$ main peaks appearing at 932.9 eV and 952.7 eV, respectively together with strong shake-up peaks at ~943 eV [34]. Moreover, some Cu atoms in these samples are in a +1 oxidation state, due to the appearance of Cu $2p_{3/2}$ and Cu $2p_{1/2}$ peaks at 931.8 and 951.7 eV [34]. The presence of Cu^{+} ions together

Table 1 – Structural properties of supports and Cu-based catalysts.

Samples	Crystallite size (nm)	Lattice parameter (Å)	Samples	BET surface area (m^2/g)	Atomic ratio[a] (%)	
					$Ce^{3+}/(Ce^{3+}+Ce^{4+})$	$Cu^{+}/(Cu^{+}+Cu^{2+})$
CT	6.8	5.40	Cu-CT	68.3	14.1	57.9
CZ	7.1	5.42	Cu-CZ	67.5	13.6	56.5
CM	6.5	5.38	Cu-CM	71.5	12.5	55.0
CeO_2	8.4	5.43	Cu–CeO_2	64.6	11.0	53.8

[a] Evaluated from XPS results of the Cu-based catalysts.

Please cite this article in press as: Ren Z, et al., A combined experimental and computational study of water-gas shift reaction over rod-shaped $Ce_{0.75}M_{0.25}O_2$ (M = Ti, Zr, and Mn) supported Cu catalysts, International Journal of Hydrogen Energy (2017), https://doi.org/10.1016/j.ijhydene.2017.10.047

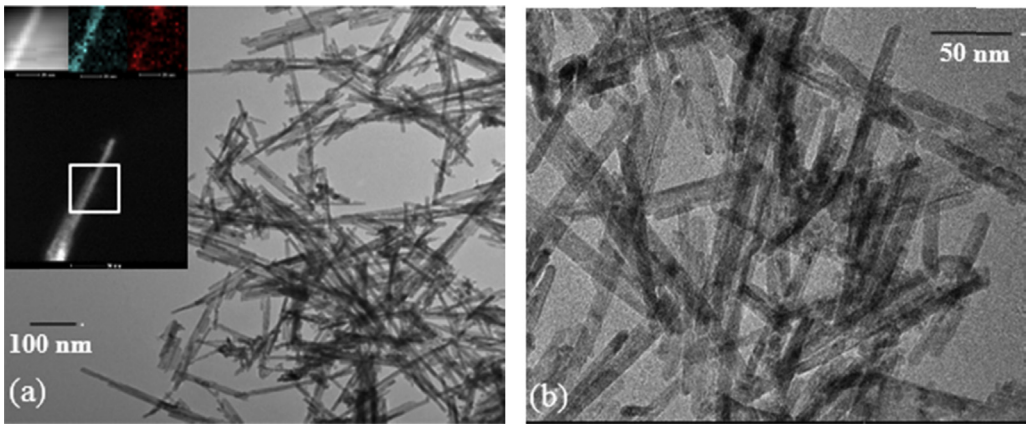

Fig. 2 – TEM images of (a) CT and (b) Cu-CT. The insets of figure (a) show an element map of CT.

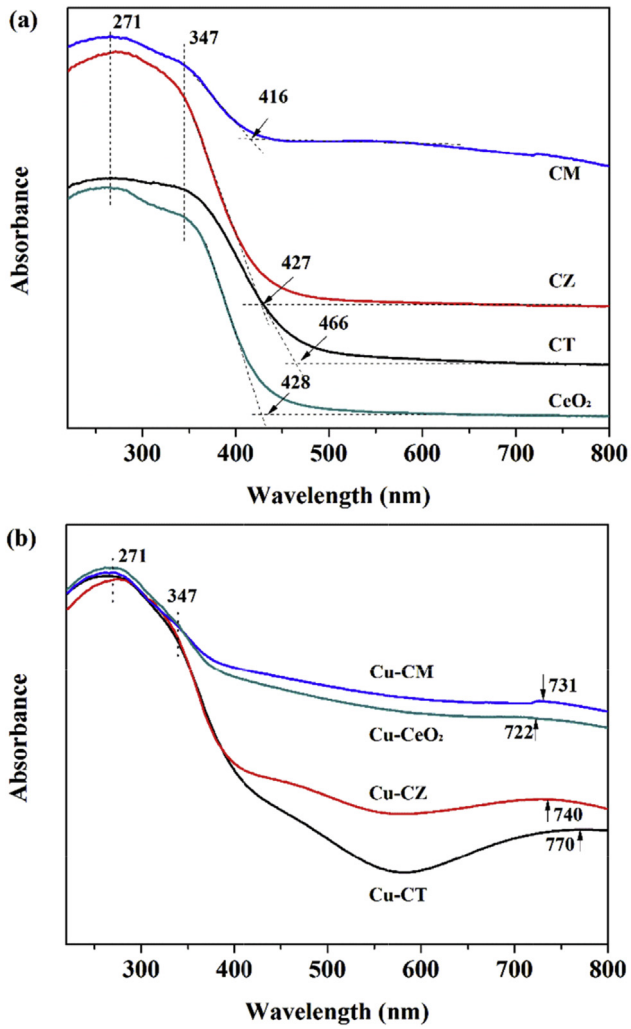

Fig. 3 – UV-vis spectra of (a) the supports and (b) Cu-based catalysts.

with the observation of Ce^{3+} species is mainly due to the redox cycle ($Cu^{2+}+Ce^{3+} \leftrightarrow Cu^{+}+Ce^{4+}$), which is claimed to be the source of the Cu-support interaction. Meanwhile, the Cu^{+} and Ce^{3+} percent contents follow a same order: Cu-CT > Cu-CZ > Cu-CM > Cu-CeO_2. (see Table 1), suggesting that high Ce^{3+} content is beneficial to the above redox cycle shifting to the right and leads to the reduction of Cu^{2+}.

In addition, the XPS spectra of Ti 3d, Zr 3d and Mn 2p for the mixed catalysts are displayed in Fig. 4c. Cu-CT exhibits two binding energy peaks of Ti $2p_{1/2}$ and Ti $2p_{3/2}$ at 464.1 and 458.4 eV, respectively, which are the characteristics of Ti^{4+} species [35]. However, the binding energies are slightly lower than those in pure TiO_2, which can be attributed to the formation of Ti^{3+} species [36]. For the Cu-CZ catalyst, the binding energy of Zr $3d_{5/2}$ is also lower than the typical binding energy of Zr^{4+} $3d_{5/2}$ (182.2 eV), conforming that the partial reduction of surface Zr^{4+} to Zr^{3+} occurred [37]. Two main peaks assigned to Mn $2p_{1/2}$ and Mn $2p_{3/2}$ can be detected in Cu-CM catalysts. The double peaks (642.0 and 643.2 eV) in the Mn $2P_{3/2}$ spectra could be assigned to Mn^{3+}, and Mn^{4+}, respectively [38]. The existence of M^{3+} (Ti^{3+}, Zr^{3+} and Mn^{3+}) implies that dual redox cycles ($Cu^{2+}+Ce^{3+} \leftrightarrow Cu^{+}+Ce^{4+}$, $M^{4+}+Ce^{3+} \leftrightarrow M^{3+}+Ce^{4+}$) are available for the mixed samples, which is further confirmed by our DFT calculations discussed later. Both of the cycles can promote each other and will result in a decrease in the energy required for the electron transfer among active copper species and supports. In addition, the electronic transfer determines the valence state of the surface Cu species, which is closely related to the adsorption and activation of CO during the WGS reaction.

The *in situ* FTIR adsorption of CO was performed at 200 °C to further understand the surface state of the copper species. When the CO is introduced into the system, all the catalysts exhibit the typical stretching bands for CO adsorption on Cu^{+} ions at 2100 cm^{-1} (Fig. 5). It is noted that the presence of reduced copper species in the XPS primarily originates from interactions between Cu^{2+} and Ce^{3+} ions through electron transfer rather than from photo-reduction. It can be found that Cu-CT and Cu-CZ catalyst exhibit stronger Cu^{+}-CO bands than Cu-CM and Cu-CeO_2, which is consistent with the higher Cu^{+} content calculated from XPS results. After purifying by He for 10 min, these two bands sharply weaken and even disappear, due to CO desorption from the Cu^{+} ions. In addition, the absorption bands of carbonate species are observed in the region of 1000–1700 cm^{-1} [14,39]. All catalysts exhibit intense bands at 1366, and 1500 cm^{-1}, attributed to the formation of

Please cite this article in press as: Ren Z, et al., A combined experimental and computational study of water-gas shift reaction over rod-shaped $Ce_{0.75}M_{0.25}O_2$ (M = Ti, Zr, and Mn) supported Cu catalysts, International Journal of Hydrogen Energy (2017), https://doi.org/10.1016/j.ijhydene.2017.10.047

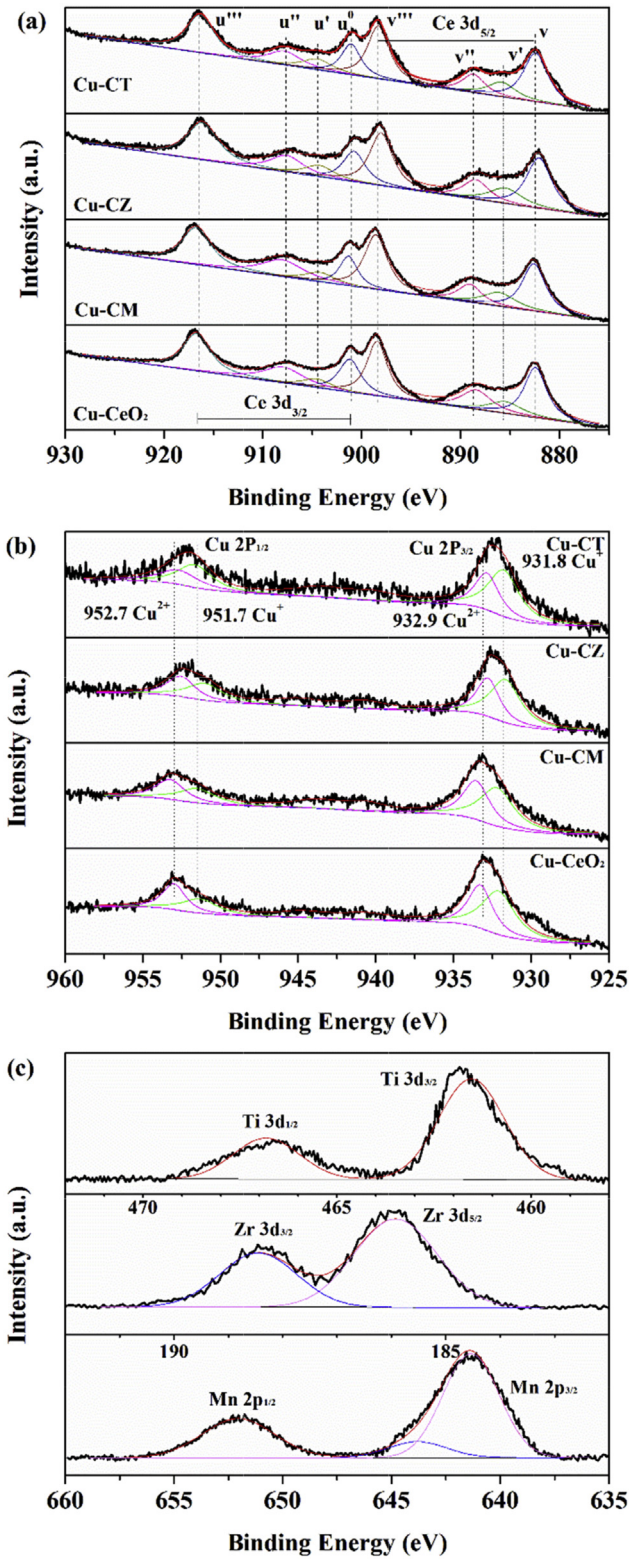

Fig. 4 – XPS spectra of (a) Ce 3d (b) Cu 2p and (c) mixed metals for the supported Cu catalysts.

monodentate-type carbonate on weak basic site. The bidentate type carbonate forming on strong basic site is simultaneously observed at 1030, 1302, and 1576 cm^{-1} [14]. These surface adsorbed carbonates suggest that CO molecules could

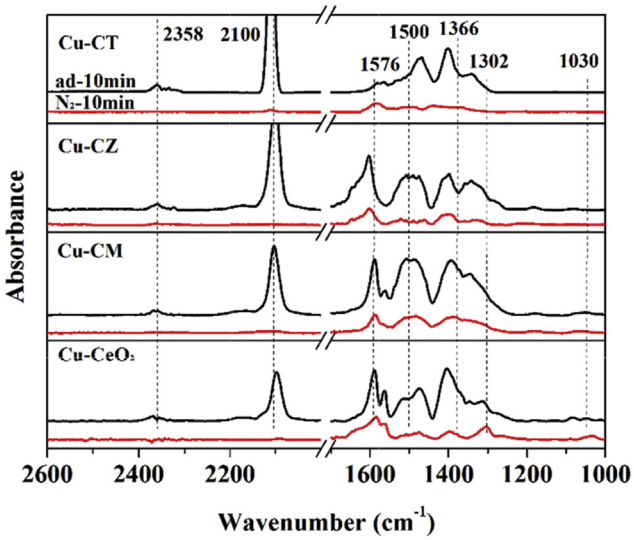

Fig. 5 – *In situ* FTIR spectra of CO adsorption on supported Cu catalysts before and after He purification (10 min) at 200 °C.

coordinate with the active oxygen species on supports. The distinctive profile in the carbonate region indicate that the site geometry and coordination environment on the catalysts surfaces are naturally different due to the introduction of foreign metal atoms.

Redox properties of the catalysts

H_2-TPR was performed to investigate the redox properties of prepared catalysts, as shown in Fig. 6. The Cu-CT show two reduction peaks below 300 °C. According to literature [8,10], the low temperature peak (denoted as peak α) is attributed to the simultaneous reduction of the adsorbed oxygen and dispersed copper oxide in proximity to the CeO_2 surface. The second peak (denoted as peak β) is related to reduction of the moderate copper oxide in close contact with CeO_2. In contrast, Cu-CZ , Cu-CM and Cu-CeO_2 display another reduction peak around 270 °C. The third shoulder peak (denoted as peak ɣ) is due to larger, aggregated copper oxide (but not detected by XRD), which weakly interacts with CeO_2. The high fraction of peak α and peak β of Cu–CT and Cu–CZ suggests the Cu should be present in a highly dispersed state. The moderate copper oxide (peak β) has a greatly positive effect on the WGS catalytic activity over supported Cu catalysts [10]. The deconvolution of H_2-TPR profiles for all catalysts indicates that the fraction of moderate copper oxide decreases following the order of Cu-CT > Cu-CZ > Cu-CM > Cu-CeO_2. With the introduction of Ti^{4+} into the CeO_2 support, the dispersed Cu species tend to present in a moderate copper oxide structure. The reduction temperature of supported CuO is much lower than that of pure CuO (320 °C) and this promoting effect originates from the interaction of copper oxide with supports. The lower the reduction temperature is, the stronger the interaction between Cu and supports will be. The differences in all of the reduction temperatures indicate that the interaction of copper oxide with supports can be ranked in

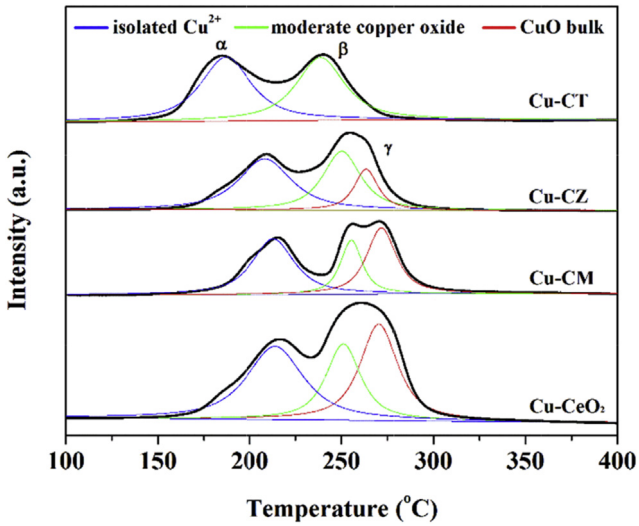

Fig. 6 – The H_2-TPR results of the supported Cu catalysts.

the order: Cu-CT > Cu-CZ > Cu-CM ≈ Cu-CeO_2. The fraction of moderate copper oxide (peak β) follows a similar sequence, indicating that the strong interaction between Cu and supports is supposed to be helpful for the dispersion of moderate copper oxide. The above mentioned results suggest that the introduction of transition metal ions into the CeO_2 supports significantly influence the dispersion and reducibility of the surface Cu species. With the best dispersion of active moderate copper oxide and strongest Cu-support interaction, the Cu-CT catalysts are supposed to show the best catalytic performance toward WGS reaction.

Catalytic activities of the catalysts

WGS reaction was performed to evaluate the catalytic performance of these catalysts. All the catalysts become active at T > 200 °C and the M mixed catalysts are clearly more active than Cu-CeO_2. The CO conversion of Cu-CT, Cu-CZ and Cu-CM arrive at thermodynamic equilibrium value even at the very high GHSV of 6000 h^{-1}; then the CO conversion decrease due to the exothermic nature of WGS reaction. Among these catalysts, Cu-CT shows the highest CO activity at the whole temperature range with the maximum CO conversion of 96.6% at T = 300 °C, which can be regarded as a promising candidate catalyst for WGS reaction. To verify the stability of the prepared Cu-based catalysts, we have performed the long-term WGS reaction test at 250 °C. Both Cu-CT and Cu-CZ catalysts have been found to be stable in 12 h without any detectable deactivation (Fig. S2), which is in good agreement with previous studies [19,40]. The activity of Cu-CM and Cu-CeO_2, however, shows a slight decrease during long-term testing. This is attributed to the weak interaction between Cu and the support (CM and ceria). The Arrhenius plots of various Cu-base catalysts in Fig. 7b show that the trend of specific rate (per gram of catalyst) is in good agreement with the provided reaction results. The apparent activation energy of the WGS reaction is obtained from the slopes of the Arrhenius plots. The calculated activation energies range from 23 kJ mol^{-1} over Cu-CT to 36 kJ mol^{-1} over Cu-CeO_2, which are in agreement

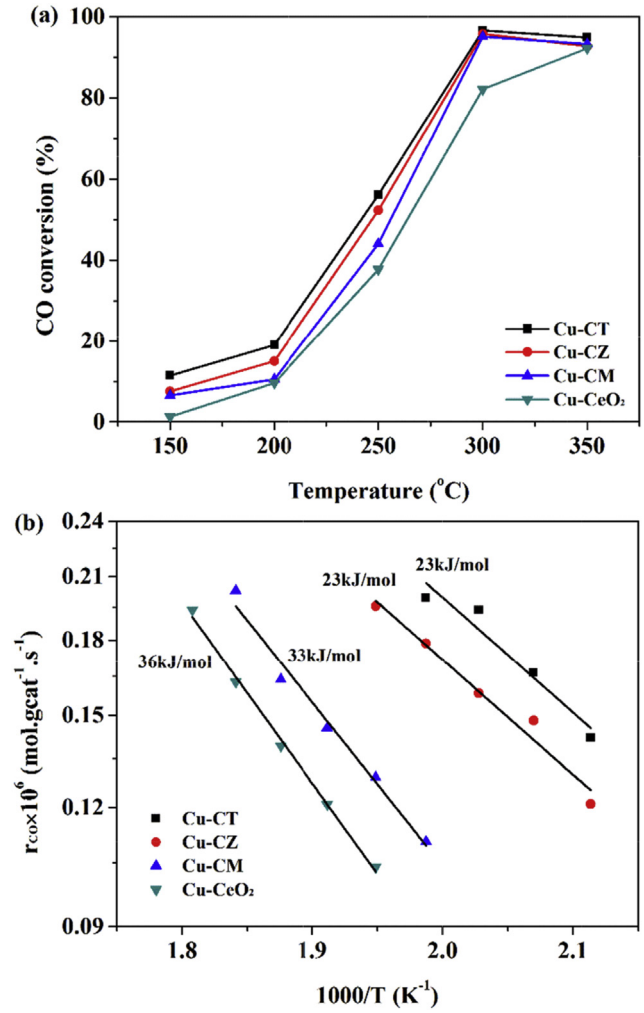

Fig. 7 – (a) Catalytic actives of supported Cu catalysts over the WGS reaction and (b) Arrhenius plot of reaction rates over supported Cu catalysts.

with the previously reported values for WGS reactions with supported Cu catalysts [19]. The difference in apparent activation energy significantly depends on the nature of the support.

On the basis of the above characterization results, the incorporating of foreign metal cations is found to significantly modify the surface coordination environments and electronic states of the catalysts, which thereby greatly affects the related final catalytic activities. As revealed by XPS, the introduction of M (Ti, Zr, Mn) into CeO_2 supports could lead to the establishment of the dual redox cycle ($Cu^{2+}+Ce^{3+} \leftrightarrow Cu^{+}+Ce^{4+}$, $M^{4+}+Ce^{3+} \leftrightarrow M^{3+}+Ce^{4+}$), which facilitates charge transfers between Cu and supports and eventually enhances the Cu-support interaction. In addition to that, the H_2-TPR suggests that copper oxide species prefer to disperse as active moderate copper oxides and strongly interact with the mixed supports, especially for the sample of Cu-CT embodying the lowest H_2-TPR peak, however, the largest peak β fraction. The dispersion difference originate from the foreign metal induced local coordination environment change on the support surface, which can be obtained from UV-vis and *in situ*

Please cite this article in press as: Ren Z, et al., A combined experimental and computational study of water-gas shift reaction over rod-shaped $Ce_{0.75}M_{0.25}O_2$ (M = Ti, Zr, and Mn) supported Cu catalysts, International Journal of Hydrogen Energy (2017), https://doi.org/10.1016/j.ijhydene.2017.10.047

FTIR results. The Cu-CT possess the highest amount of active Cu oxide species as well as the strongest Cu-support interaction, which constitute an important factor resulting in the highest WGS activity. Therefore, it can be concluded that the outstanding activity of Cu-CT is related to strong Cu-support interaction resulting in lower activation energy and abundant moderate copper species possessing more active sites.

DFT calculations

To gain a further insight into the role of mixing foreign metal (M) in the catalytic performance of WGS over supported Cu catalysts, periodic DFT calculations were carried out. $Ce_{0.75}M_{0.25}O_2$ is modeled using a cubic fluorite CeO_2 structure where the substitution of one Ce atom in the cell with an M (Zr, Ti and Mn) atom gives an overall M atom concentration of 25% (Fig. S3). The predicted lattice constants for pure, Zr-mixed, and Ti-mixed CeO_2 are 5.44, 5.36, and 5.31 Å, respectively, which is in agreement with our experimental values (Table 1). The prepared CeO_2 rods selectively exposing (100) and (110) crystal planes has been confirmed by HRTEM observations in previous studies [13–16]. After the incorporation of Zr^{4+} and Ti^{4+} into the lattice, the CeO_2 rods still inherit their authentic crystalline structure, which was confirmed by our XRD results. So the pure CeO_2(110) slab and corresponding Zr, Ti mixed slabs are considered for modeling support surfaces and with the top view being shown in Fig. 8a–c. For the stoichiometric CeO_2 (110) surface, the Ce atoms in the surface layer are coordinated to two pairs of surface oxygen atoms (O_s) and a pair of subsurface oxygen atoms (O_{sub}); each O_s is coordinated to two surface and one subsurface Ce atom. The optimized CeO_2(110) surface has a Ce-O_s bond length equal to 2.32 Å. For the $Ce_{0.75}Zr_{0.25}O_2$(110) surface, the Ce atom has relaxed to form Ce-O_s bond of 2.37 and Zr-O_s bond of 2.21 Å. The change in Ce-O_s bond is attributed to slight distortions in the atomic structure around the Zr atoms. In the $Ce_{0.75}Ti_{0.25}O_2$(110) structure, the O_s in the closest distance to the Ti atoms can move away their initial lattice site, resulting a short Ti-O_s bond length of 2.05 Å and a long Ce-O_s bond length of 2.50 Å. The incorporation of Ti produces a strong geometric distortion of the oxygen lattice, which can be attributed to its small ionic radius. In general, the mixed second metal atom in the CeO_2 lattice will distort the initial structure of the host oxide to build their most favorable coordination environment, which is in agreement with our XRD and UV results.

Oxygen vacancies on the oxide support surface are well recognized to play a key role in the activity of WGS reaction [27]. The vacancy sites (O_v) are generated by removing surface oxygen atoms, as in Fig. 8d–f. The O_s near to the O_v moves from its lattice site, thus bridging two neighboring cations (surface M or Ce atom) and then fills the vacancy. This split vacancy structure is in agreement with results previously reported in the literature [40]. Similar to the stoichiometric surfaces, the bridging O_s migrates towards the small M atoms, which results in the Zr-O_s bond length of 1.98 Å and the Ti-O_s bond length of 1.79 Å. It is worth noting that these bonds in the reduced surfaces become shorter than those in the vacancy free surfaces, as the mixed M atoms attempt to maximize the coordination to oxygen. The O_v formation energy is calculated by

$$\Delta E_{O-Vac} = \left(E_{slab/O_v} + 1/2E_{O_2}\right) - E_{slab}$$

where E_{slab} and $E_{slab/Ov}$ are the total energy of the stoichiometric and reduced surfaces, E_{O2} is the energy of a gas-phase

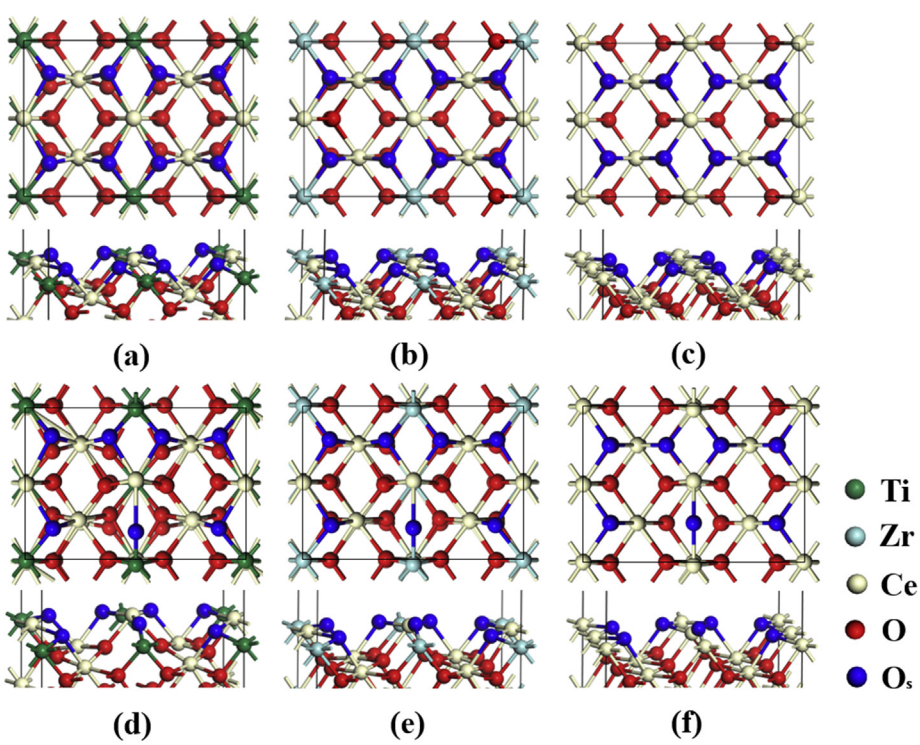

Fig. 8 – Top and side view of the optimized configurations of (a–c) stoichiometric (110) surface and (d–f) reduced (110) surface.

Please cite this article in press as: Ren Z, et al., A combined experimental and computational study of water-gas shift reaction over rod-shaped $Ce_{0.75}M_{0.25}O_2$ (M = Ti, Zr, and Mn) supported Cu catalysts, International Journal of Hydrogen Energy (2017), https://doi.org/10.1016/j.ijhydene.2017.10.047

O_2 in vacuum. The energy required for the formation of the surface O_v on CeO_2(110) is calculated to be 165 kJ mol^{-1}. This value is in agreement with that of 159 kJ mol^{-1} calculated by Cheng et al. [40] The formation energies of surface O_v are calculated to be 104 and 62 kJ mol^{-1} for Zr- and Ti-mixed surface. The smaller O_v formation energies for mixed ceria surfaces suggest that the O_v formation is much more favored by mixing Zr and Ti metals. This confirms our experimental observations.

The reaction mechanism of WGS reaction over supported metal catalysts is still in dispute. Although various reaction mechanisms such as simply redox mechanism, formate intermediates mechanism, and carboxyl-mediated mechanism had been proposed [4], the adsorption of CO is unquestionably the first step in all proposed reaction mechanisms. CO molecule generally prefers to adsorb on the supported metal nanoparticles rather than on the support surfaces. The experimental results indicate that copper are highly dispersed on all support surfaces. The moderate copper species has a greatly positive effect on the WGS catalytic activity over supported Cu catalysts, instead of the large, aggregated copper particles. As previously reported [41,42], the Cu_4 cluster can be introduced onto the CeO_2 slab to model the supported high dispersed Cu particle, which provided a good description of metal-CeO_2 interface and Cu-support interaction. Thus, the supported Cu catalysts are represented by a Cu_4 cluster over various Ce-based supports in the present work. As depicted in Fig. 9a–c, the Cu_4 clusters remain in the tetrahedral shape upon adsorption onto the support surfaces through the Cu-O bonds. The calculated binding energies of the Cu_4 cluster on $Ce_{0.75}Ti_{0.25}O_2$(110), $Ce_{0.75}Zr_{0.25}O_2$(110) and CeO_2(110) are −264, −209 and −192 kJ mol^{-1}, respectively. Therefore, the Cu-support interaction follows the order of Cu-CT > Cu-CZ > Cu-CeO_2, which is consistent with our experimental results derived from H_2-TPR. It is noted that the CO is apt to bind to the top site of the supported Cu_4 cluster (Fig. 9d–f) with adsorption energies of −117, −103, and −86 kJ mol^{-1} for CO-Cu_4–$Ce_{0.75}Ti_{0.25}O_2$(110), CO-Cu_4-$Ce_{0.75}Zr_{0.25}O_2$(110) and CO-Cu_4–CeO_2(110), respectively. Again, the Cu-CT provides the strongest CO adsorption. The calculated frequencies for CO on the Cu_4-$Ce_{0.75}Ti_{0.25}O_2$(110), Cu_4-$Ce_{0.75}Zr_{0.25}O_2$(110) and Cu_4-CeO_2(110) are 2082, 2080 and 2076 cm^{-1}, which correspond to the CO adsorption bands at 2100 cm^{-1} in Fig. 5. To understand how the mixed second metal in the support affect the oxidation state Cu and CO adsorption, we performed a Bader charge and density of states (DOS) analysis on the optimized catalyst models. The Bader charges of Cu_4 on $Ce_{0.75}Ti_{0.25}O_2$(110), $Ce_{0.75}Zr_{0.25}O_2$(110) and CeO_2(110) are +0.94, +0.91 and + 0.89 |e|, respectively. Similar to the adsorption on the supported Au [43], CO adsorption energies are related to the diverse oxidation state of supported Cu catalysts: more positive charge on Cu resulted in stronger CO adsorption. When Cu_4 cluster adsorbs on the support surfaces, the filled Ce-4f band appears in the energy range labeled "A" near the Fermi level, which results from the reduction of Ce^{4+} to Ce^{3+} ion. The overlap of Cu-d states and the O-p states reveals that the electron transfer from Cu_4 to support is through the Cu-O bond as shown in Fig. 10a–c displaying the charge density differences. Compared to Cu_4-CeO_2(110), the Ti, Zr mixed catalysts display two new features of B and C at 2–4 eV. The feature B is related to the interactions of O-p states, Ce-f states, and Ti-d states. The Ce-O–Zr interaction results in the C feature in Fig. 10e. It is noticeable that the no overlap of Cu-d states and the Ti-d (or Zr-d) states is observed at 2–4 eV, indicating that there is little

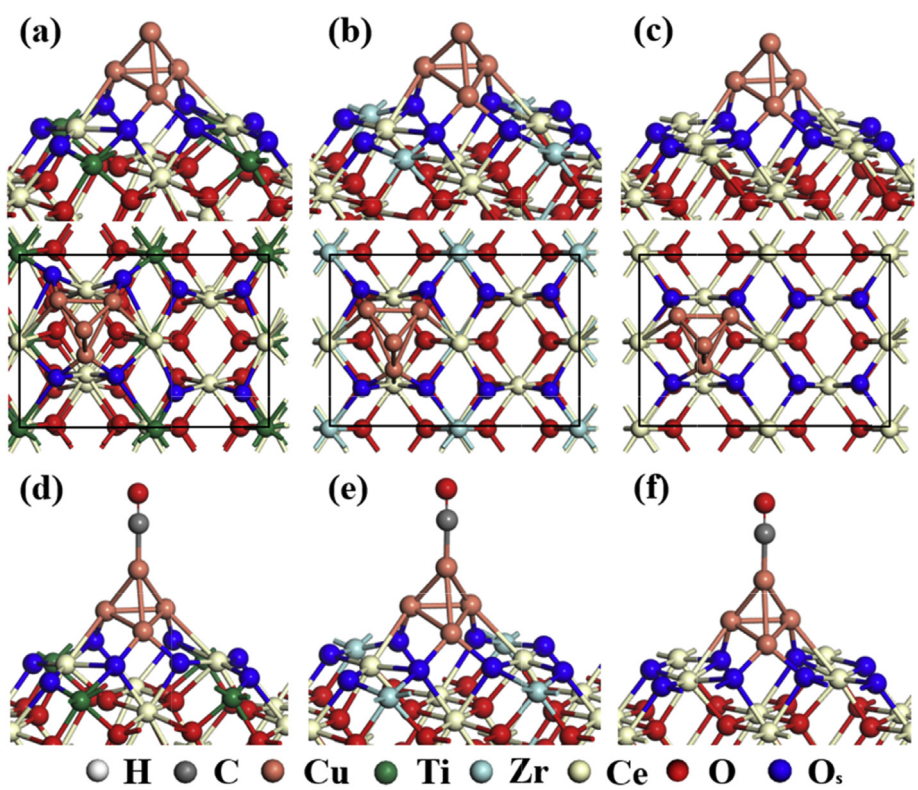

Fig. 9 – The optimized configurations of (a–c) supported Cu_4 cluster and (d–f) CO adsorption.

Please cite this article in press as: Ren Z, et al., A combined experimental and computational study of water-gas shift reaction over rod-shaped $Ce_{0.75}M_{0.25}O_2$ (M = Ti, Zr, and Mn) supported Cu catalysts, International Journal of Hydrogen Energy (2017), https://doi.org/10.1016/j.ijhydene.2017.10.047

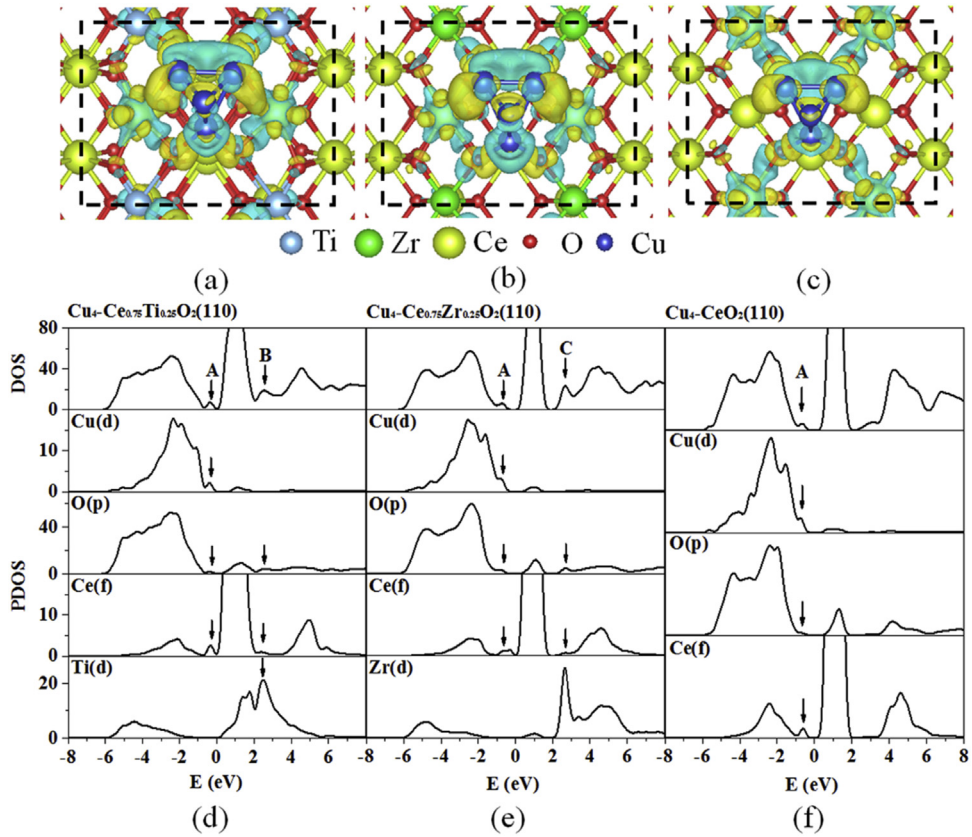

Fig. 10 – (a–c) Electronic density difference upon adsorption of Cu_4 clusters on support surfaces (yellow and blue colors represent increasing and decreasing electron densities, respectively); (d–f) total DOS and atom-resolved projected DOS analysis. (For interpretation of the references to colour in this figure legend, the reader is referred to the web version of this article.)

electron transfer from Cu to Ti, Zr. On the basis of DOS and Bader charge analysis, it can be concluded that the supported Cu_4 cluster loses some of electrons from 3d orbital, which is mainly transferred to the 4f orbital of Ce ions in the pure CeO_2 support. However, upon the mixing with Ti and Zr, more electrons would transfer from the supported Cu cluster to the Ce in the support. This is also consistent with our observation from XPS results.

H_2O is most likely to adsorb on the oxide support or the metal-support interface. Adsorbed water then further dissociates forming two surface OH groups [27,44]. The carboxyl (COOH) formation from adsorbed CO and OH at the interface between the metal cluster and the oxide support had been proposed to be rate-limiting step in the WGS reaction. The synergistic effects at the copper-ceria interface facilitate the formation of the COOH intermediate, thus increasing thus the catalytic activity [44,45]. Therefore, the observed different WGS activities on various mixed ceria-based supported Cu catalyst could be rationally explained by the COOH formation on the Cu-support interface. As shown in Fig. 11, the COOH formation step on Cu_4-CeO_2(110) starts from the CO adsorbed on a Cu site and OH bridge-bonded to the Ce_s and Cu. The formation of COOH proceeds via the break of O-Ce bond and the formation of C-O bond (Fig. 11). The activation energy for this step on Cu_4-CeO_2(110) is 46 kJ mol^{-1} and this reaction is

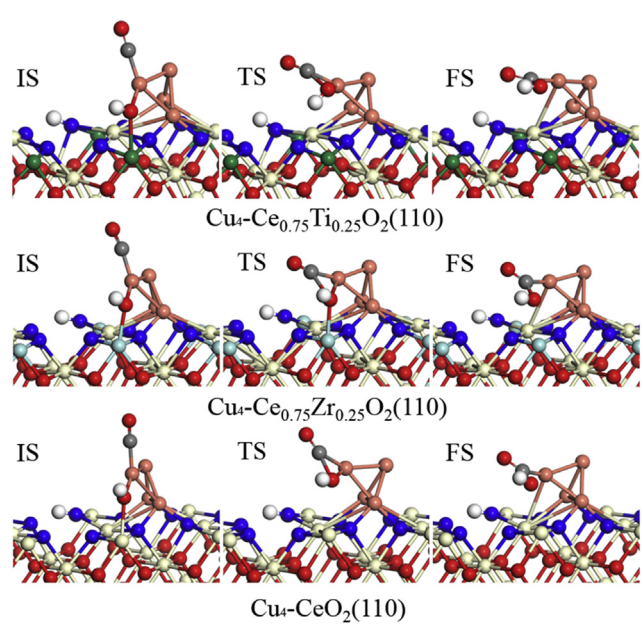

Fig. 11 – The configurations of the optimized IS, TS and FS structures.

Please cite this article in press as: Ren Z, et al., A combined experimental and computational study of water-gas shift reaction over rod-shaped $Ce_{0.75}M_{0.25}O_2$ (M = Ti, Zr, and Mn) supported Cu catalysts, International Journal of Hydrogen Energy (2017), https://doi.org/10.1016/j.ijhydene.2017.10.047

endothermic with a reaction energy of 35 kJ mol^{-1}. This calculation result is comparable to those on Pt-CeO_2 [46] and Au-CeO_2 [47]. In the similar way, we calculate the COOH formation over mixed oxide support Cu catalysts. The COOH formation is promoted on the $Ce_{0.75}Ti_{0.25}O_2$(110) and Cu_4-$Ce_{0.75}Zr_{0.25}O_2$(110) surfaces with lower activation energies of 29 and 32 kJ mol^{-1}. Compared to the Cu_4-CeO_2(110) surface, the COOH formation step is found to be less endothermic with the calculated reaction energies of 22 and 20 kJ mol^{-1} on the Ti, Zr mixed ceria supported Cu catalysts, respectively. It is noted that the DFT calculated activation energy for the COOH formation on Cu_4-$Ce_{0.75}Ti_{0.25}O_2$(110) is 29 kJ mol^{-1}, which is also close to the experimental measured value of 23 kJ mol^{-1} in this work. The low activation energy for the Ti and Zr mixed ceria systems accounts for the high activity of WGS reaction over supported Cu catalysts.

Conclusions

In the present work, Ti, Zr and Mn mixed ceria nano-rods were synthesized by hydrothermal method. These mixed ceria-based solid solution materials were then used as the Cu catalyst support for WGS reaction. The surface chemical properties of the obtained catalysts are found to be distinguish from each other due to incorporation of different foreign metals (Ti, Zr and Mn). The Ti mixed oxides provide the best option for the well dispersed Cu species, the largest amount of moderate copper oxide, as well as the strongest Cu-support interaction, leading to the highest WGS activity among all investigated ceria-based mixed supports. Further theoretical modeling calculations suggest that the introduction of Ti atoms into CeO_2 promotes oxygen vacancies formation as well as CO adsorption on supported Cu clusters. Most importantly, the Ti mixed oxide supported Cu catalyst shows lower activation energy in the COOH formation, which is supposed to be the rate-controlling reaction step in WGS. In combination of experimental and DFT calculation results, we find that incorporation of second foreign metal is an effective strategy to tailor the surface chemical properties of the CeO_2 supports and further improve the catalytic activity of the supported Cu catalysts, in particular for the redox reactions like WGS where the chemical and physical properties of both the support and the metal catalyst play the important role in the reaction.

Acknowledgements

This work was financially supported by the National Natural Science Foundation of China (No. 21476012, 21571012, and 91534201). Z. Ren appreciates the joint Ph.D. scholarship support from the China Scholarship Council. The computing time was also granted by a scientific theme user proposal in the William R. Wiley Environmental Molecular Sciences Laboratory (EMSL), which is a U.S. Department of Energy national scientific user facility located at PNNL in Richland, Washington. D. Mei is supported by the US Department of Energy, Office of Basic Energy Sciences, Division of Chemical Sciences, Geosciences & Biosciences.

Appendix A. Supplementary data

Supplementary data related to this article can be found at https://doi.org/10.1016/j.ijhydene.2017.10.047.

REFERENCES

[1] Santos JL, Reina TR, Ivanova S, Centeno MA, Odriozola JA. Gold promoted Cu/ZnO/Al_2O_3 catalysts prepared from hydrotalcite precursors: advanced materials for the WGS reaction. Appl Catal B 2017;201:310–7.
[2] LeValley TL, Richard AR, Fan MH. The progress in water gas shift and steam reforming hydrogen production technologies – a review. Int J Hydrogen Energy 2014;39:16983–7000.
[3] Graciani J, Sanz JF. Designing a new generation of catalysts: water gas shift reaction example. Catal Today 2015;240:214–9.
[4] Kubacka A, Fernandez-Garcia M, Martinez-Arias A. Catalytic hydrogen production through WGS or steam reforming of alcohols over Cu, Ni and Co catalysts. Appl Catal A 2016;518:2–17.
[5] Jeong DW, Jang WJ, Shim JO, Han WB, Roh HS, Jung UH, et al. Low-temperature water-gas shift reaction over supported Cu catalysts. Renew Energy 2014;65:102–7.
[6] Boisen A, Janssens TVW, Schumacher N, Chorkendorff I, Dahl S. Support effects and catalytic trends for water gas shift activity of transition metals. J Mol Catal A Chem 2010;315:163–70.
[7] Jeong DW, Na HS, Shim JO, Jang WJ, Roh HS, Jung UH, et al. Hydrogen production from low temperature WGS reaction on co-precipitated Cu-CeO_2 catalysts: an optimization of Cu loading. Int J Hydrogen Energy 2014;39:9135–42.
[8] Li L, Song L, Chen C, Zhang Y, Zhan Y, Lin X, et al. Modified precipitation processes and optimized copper content of CuO–CeO_2 catalysts for water-gas shift reaction. Int J Hydrogen Energy 2014;39:19570–82.
[9] Sagata K, Kaneda Y, Yamaura H, Kobayashi S, Yahiro H. Influence of coexisting Al_2O_3 on the activity of copper catalyst for water-gas-shift reaction. Int J Hydrogen Energy 2014;39:20639–45.
[10] Chen C, Ruan C, Zhan Y, Lin X, Zheng Q, Wei K. The significant role of oxygen vacancy in Cu/ZrO_2 catalyst for enhancing water-gas-shift performance. Int J Hydrogen Energy 2014;39:317–24.
[11] Zhang Y, Chen C, Lin X, Li D, Chen X, Zhan Y, et al. CuO/ZrO_2 catalysts for water-gas shift reaction : nature of catalytically active copper species. Int J Hydrogen Energy 2014;39:3746–54.
[12] Wu K, Sun LD, Yan CH. Recent progress in well-controlled synthesis of ceria-based nanocatalysts towards enhanced catalytic performance. Adv Energy Mater 2016;6.
[13] Hu Z, Liu XF, Meng DM, Guo Y, Guo YL, Lu GZ. Effect of ceria crystal plane on the physicochemical and catalytic properties of Pd/ceria for CO and propane oxidation. ACS Catal 2016;6:2265–79.
[14] Liu L, Yao Z, Deng Y, Gao F, Liu B, Dong L. Morphology and crystal-plane effects of nanoscale ceria on the activity of CuO/CeO_2 for NO reduction by CO. ChemCatChem 2011;3:978–89.
[15] Ma ZW, Zhao SL, Pei XP, Xiong XM, Hu B. New insights into the support morphology-dependent ammonia synthesis activity of Ru/CeO_2 catalysts. Catal Sci Technol 2017;7:191–9.
[16] Si R, Flytzani-Stephanopoulos M. Shape and crystal-plane effects of nanoscale ceria on the activity of Au-CeO_2 catalysts

for the water-gas shift reaction. Angew Chem 2008;120:2926–9.
[17] Li Y, Shen W. Morphology-dependent nanocatalysts: rod-shaped oxides. Chem Soc Rev 2014;43:1543–74.
[18] Fraccari EP, D'Alessandro O, Sambeth J, Baronetti G, Mariño F. Ce-Mn mixed oxides as supports of copper- and nickel-based catalysts for water-gas shift reaction. Fuel Process Technol 2014;119:67–73.
[19] Jeong D-W, Na H-S, Shim J-O, Jang W-J, Roh H-S. A crucial role for the CeO_2-ZrO_2 support for the low temperature water gas shift reaction over Cu-CeO_2-ZrO_2 catalysts. Catal Sci Technol 2015;5:3706–13.
[20] Myung JH, Shin TH, Huang XB, Carins G, Irvine JTS. Enhancement of redox stability and electrical conductivity by doping various metals on ceria, $Ce_{1-x}M_xO_{2-\delta}$ (M = Ni, Cu, Co, Mn, Ti, Zr). Int J Hydrogen Energy 2015;40:12003–8.
[21] Petallidou KC, Polychronopoulou K, Boghosian S, Garcia-Rodriguez S, Efstathiou AM. Water-gas shift reaction on Pt/$Ce_{1-x}Ti_xO_{2-\delta}$: the effect of Ce/Ti ratio. J Phys Chem C 2013;117:25467–77.
[22] Chen W-T, Chen K-B, Wang M-F, Weng S-F, Lee C-S, Lin M. Enhanced catalytic activity of $Ce_{1-x}M_xO_2$ (M=Ti, Zr, and Hf) solid solution with controlled morphologies. Chem Commun 2010;46:3286–8.
[23] Si R, Raitano J, Yi N, Zhang LH, Chan SW, Flytzani-Stephanopoulos M. Structure sensitivity of the low-temperature water-gas shift reaction on Cu-CeO_2 catalysts. Catal Today 2012;180:68–80.
[24] Kresse G, Furthmuller J. Efficiency of ab–initio total energy calculations for metals and semiconductors using a plane-wave basis set. Comp Mater Sci 1996;6:15–50.
[25] Kresse G, Furthmuller J. Efficient iterative schemes for ab initio total-energy calculations using a plane-wave basis set. Phys Rev B 1996;54:11169–86.
[26] Perdew JP, Burke K, Ernzerhof M. Generalized gradient approximation made simple. Phys Rev Lett 1996;77:3865–8.
[27] Aranifard S, Ammal SC, Heyden A. On the importance of metal-oxide interface sites for the water-gas shift reaction over Pt/CeO_2 catalysts. J Catal 2014;309:314–24.
[28] Henkelman G, Uberuaga BP, Jónsson H. A climbing image nudged elastic band method for finding saddle points and minimum energy paths. J Chem Phys 2000;113:9901–4.
[29] Li HJ, Qi GS, Tana, Zhang XJ, Huang XM, Li W, et al. Low-temperature oxidation of ethanol over a $Mn_{0.6}Ce_{0.4}O_2$ mixed oxide. Appl Catal B 2011;103:54–61.
[30] Yao X, Tang C, Ji Z, Dai Y, Cao Y, Gao F, et al. Investigation of the physicochemical properties and catalytic activities of $Ce_{0.67}M_{0.33}O_2$ (M= Zr^{4+}, Ti^{4+}, Sn^{4+}) solid solutions for NO removal by CO. Catal Sci Technol 2013;3:688–98.
[31] Liu L, Yao Z, Liu B, Dong L. Correlation of structural characteristics with catalytic performance of CuO/CexZr$_{1-x}O_2$ catalysts for NO reduction by CO. J Catal 2010;275:45–60.
[32] Zabilskiy M, Djinovic P, Erjavec B, Drazic G, Pintar A. Small CuO clusters on CeO_2 nanospheres as active species for catalytic N_2O decomposition. Appl Catal B 2015;163:113–22.
[33] Cheng X, Zhu A, Zhang Y, Wang Y, Au C, Shi C. A combined DRIFTS and MS study on reaction mechanism of NO reduction by CO over NiO/CeO_2 catalyst. Appl Catal B 2009;90:395–404.
[34] Tonelli F, Gorriz O, Tarditi A, Cornaglia L, Arrua L, Abello MC. Activity and stability of a CuO/CeO_2 catalyst for methanol steam reforming. Int J Hydrogen Energy 2015;40:13379–87.
[35] Yao X, Zhang L, Li L, Liu L, Cao Y, Dong X, et al. Investigation of the structure, acidity, and catalytic performance of CuO/$Ti_{0.95}Ce_{0.05}O_2$ catalyst for the selective catalytic reduction of NO by NH_3 at low temperature. Appl Catal B 2014;150:315–29.
[36] Seo PW, Cho SP, Hong SH, Hong SC. The influence of lattice oxygen in titania on selective catalytic reduction in the low temperature region. Appl Catal A 2010;380:21–7.
[37] Zhang Y, Zhan Y, Chen C, Cao Y, Lin X, Zheng Q. Highly efficient Au/ZrO_2 catalysts for low-temperature water-gas shift reaction: effect of pre-calcination temperature of ZrO_2. Int J Hydrogen Energy 2012;37:12292–300.
[38] Gao R, Zhang D, Maitarad P, Shi L, Rungrotmongkol T, Li H, et al. Morphology-dependent properties of MnO_x/ZrO_2-CeO_2 nanostructures for the selective catalytic reduction of NO with NH_3. J Phys Chem C 2013;117:10502–11.
[39] Chen S, Cao T, Gao Y, Li D, Xiong F, Huang W. Probing surface structures of CeO_2, TiO_2, and Cu_2O nanocrystals with CO and CO_2 chemisorption. J Phys Chem C 2016;120:21472–85.
[40] Cheng Z, Lo CS. Mechanistic and microkinetic analysis of CO_2 hydrogenation on ceria. Phys Chem Chem Phys 2016;18:7987–96.
[41] Yang Z, Xie L, Ma D, Wang G. Origin of the high activity of the ceria-supported copper catalyst for H_2O dissociation. J Phys Chem C 2011;115:6730–40.
[42] Piotrowski MJ, Tereshchuk P, Da Silva JL. Theoretical investigation of small transition-metal clusters supported on the CeO_2(111) surface. J Phys Chem C 2014;118:21438–46.
[43] Song WY, Hensen EJM. Structure sensitivity in CO oxidation by a single Au atom supported on ceria. J Phys Chem C 2013;117:7721–6.
[44] Plata JJ, Graciani J, Evans J, Rodriguez JA. Sanz JFn. Cu deposited on CeO_x-modified TiO_2(110): synergistic effects at the metal-oxide interface and the mechanism of the WGS reaction. ACS Catal 2016;6:4608–15.
[45] Aranifard S, Ammal SC, Heyden A. On the importance of the associative carboxyl mechanism for the water-gas shift reaction at Pt/CeO_2 interface sites. J Phys Chem C 2014;118:6314–23.
[46] Song W, Hensen EJ. Mechanistic aspects of the water–gas shift reaction on isolated and clustered Au atoms on CeO_2 (110): a density functional theory study. ACS Catal 2014;4:1885–92.
[47] Chen Y, Wang HF, Burch R, Hardacre C, Hu P. New insight into mechanisms in water-gas-shift reaction on Au/CeO_2(111): a density functional theory and kinetic study. Faraday Discuss 2011;152:121–33.

Please cite this article in press as: Ren Z, et al., A combined experimental and computational study of water-gas shift reaction over rod-shaped $Ce_{0.75}M_{0.25}O_2$ (M = Ti, Zr, and Mn) supported Cu catalysts, International Journal of Hydrogen Energy (2017), https://doi.org/10.1016/j.ijhydene.2017.10.047